GEOCHEMISTRY

Chronology of martian breccia NWA 7034 and the formation of the martian crustal dichotomy

William S. Cassata,[1]* Benjamin E. Cohen,[2,3] Darren F. Mark,[2,4] Reto Trappitsch,[1] Carolyn A. Crow,[1] Joshua Wimpenny,[1] Martin R. Lee,[3] Caroline L. Smith[3,5]

Martian meteorite Northwest Africa (NWA) 7034 and its paired stones are the only brecciated regolith samples from Mars with compositions that are representative of the average martian crust. These samples therefore provide a unique opportunity to constrain the processes of metamorphism and alteration in the martian crust, which we have investigated via U-Pu/Xe, $^{40}Ar/^{39}Ar$, and U-Th-Sm/He chronometry. U-Pu/Xe ages are comparable to previously reported Sm-Nd and U-Pb ages obtained from NWA 7034 and confirm an ancient (>4.3 billion years) age for the source lithology. After almost 3000 million years (Ma) of quiescence, the source terrain experienced several hundred million years of thermal metamorphism recorded by the K-Ar system that appears to have varied both spatially and temporally. Such protracted metamorphism is consistent with plume-related magmatism and suggests that the source terrain covered an areal extent comparable to plume-fed edifices (hundreds of square kilometers). The retention of such expansive, ancient volcanic terrains in the southern highlands over billions of years suggests that formation of the martian crustal dichotomy, a topographic and geophysical divide between the heavily cratered southern highlands and smoother plains of the northern lowlands, likely predates emplacement of the NWA 7034 source terrain—that is, it formed within the first ~100 Ma of planetary formation.

INTRODUCTION

Northwest Africa (NWA) 7034 and its paired stones (NWA 7475, NWA 7533, NWA 7906, NWA 7907, NWA 8114, NWA 8171, NWA 8674, NWA 10922, NWA 11220, NWA 11522, and Rabt Sbayta 003) are the oldest and most diverse of the martian meteorites (data obtained from NWA 7034 and its paired stones are not distinguished in the text). These polymict regolith breccias contain predominantly igneous clasts and mineral fragments, with minor impact melt and proto-breccia clasts (*1*). NWA 7034 and its pairings are the only martian meteorites identified to date with major element compositions that are comparable to the average martian crust (*2*). Moreover, the stones contain secondary alteration minerals associated with aqueous processes that may have been widespread in the martian crust [for example, the studies of Liu *et al.* (*3*) and Wittmann *et al.* (*4*)]. As such, better constraints on the thermal history of NWA 7034 may shed light on the nature and extent of near-surface metamorphism and the duration and temperatures of aqueous alteration on Mars.

Igneous clasts and matrix minerals in NWA 7034 define a Sm-Nd isochron age of 4420 ± 70 million years (Ma), which suggests the various lithological components formed contemporaneously (*5*). U-Pb ages obtained from mineral fragments define two populations of ages. "Old" ages obtained from baddeleyite and zircon crystals range from 4428 ± 50 to 4311 ± 52 Ma (Fig. 1) (*2*, *6*–*8*). "Young" ages obtained from phosphates and metamict zircons range from 1712 ± 170 to 1345 ± 47 Ma (Fig. 1) (*2*, *6*–*9*). Although the old U-Pb and Sm-Nd ages are statistically indistinguishable, the young zircon and phosphate ages indicate that one or more metamorphic events occurred at ~1700 to 1300 Ma, resulting in partial resetting of the U-Pb system. K-Ar and $^{40}Ar/^{39}Ar$ ages of 1560 Ma (*10*) and 1285 ± 8 Ma (*11*), respectively, further attest to thermal processing at that time (Fig. 1).

Younger radiometric ages (1700 to 1300 Ma) have generally been interpreted as dating a single metamorphic event associated with brecciation [for example, see Nyquist *et al.* (*5*) and McCubbin *et al.* (*6*)]. However, the ages appear to differ beyond analytical uncertainties, and it is unclear whether the disparity reflects systematic uncertainties in the data sets or, alternatively, a more protracted brecciation or metamorphic history. Further complicating the chronology, NWA 7034 yields an apparent U-Th/He age of 170 Ma (*10*). The U-Th-Sm/He system is unlikely to have been reset during ejection because NWA 7034 is only shocked to 5 to 15 GPa (discussed in more detail below) (*4*). It thus appears that at least one additional metamorphic event may have occurred between ~1300 Ma and ejection (*12*).

Here, we report $^{40}Ar/^{39}Ar$, U-Th-Sm/He, and U-Pu/Xe ages obtained from whole-rock fragments and mineral separates to better constrain the impact and metamorphic history of NWA 7034. The chronometers span a wide range of closure temperatures and are therefore sensitive to different metamorphic conditions (*13*–*15*). To explore clast-to-clast variations in metamorphic ages, we selected a total of 4 feldspar mineral separates and 13 individual matrix/clast chips from visibly monomict fragments for $^{40}Ar/^{39}Ar$ measurements. In addition, we measured He, Ne, Ar, Kr, and Xe isotopes to better constrain the conditions of brecciation and ejection from Mars. Collectively, the data suggest that metamorphism at 1500 to 1200 Ma is associated with protracted magmatic activity, and brecciation occurred much later (after ~225 Ma). A corollary of this interpretation is that the ancient source terrain of NWA 7034 was preserved essentially intact since emplacement, likely requiring that the martian crustal dichotomy formed before ~4400 Ma.

MATERIALS AND METHODS

Whole-rock fragments and mineral separates were analyzed for $^{40}Ar/^{39}Ar$ chronometry in the Livermore Noble Gas Lab at Lawrence Livermore National Laboratory (LLNL) and the Natural Environment Research Council (NERC) Argon Isotope Facility, Scottish Universities Environmental Research Centre (SUERC). Aliquots analyzed at LLNL

[1]Nuclear and Chemical Sciences Division, Lawrence Livermore National Laboratory, Livermore, CA 94550, USA. [2]Isotope Geoscience Unit, Scottish Universities Environmental Research Centre, Rankine Avenue, East Kilbride, G75 0QF, UK. [3]School of Geographical and Earth Sciences, University of Glasgow, G12 8QQ, UK. [4]Department of Earth and Environmental Sciences, University of St. Andrews, St. Andrews, KY16 9AJ, UK. [5]Department of Earth Sciences, Natural History Museum, London, SW7 5BD, UK.
*Corresponding author. Email: cassata2@llnl.gov

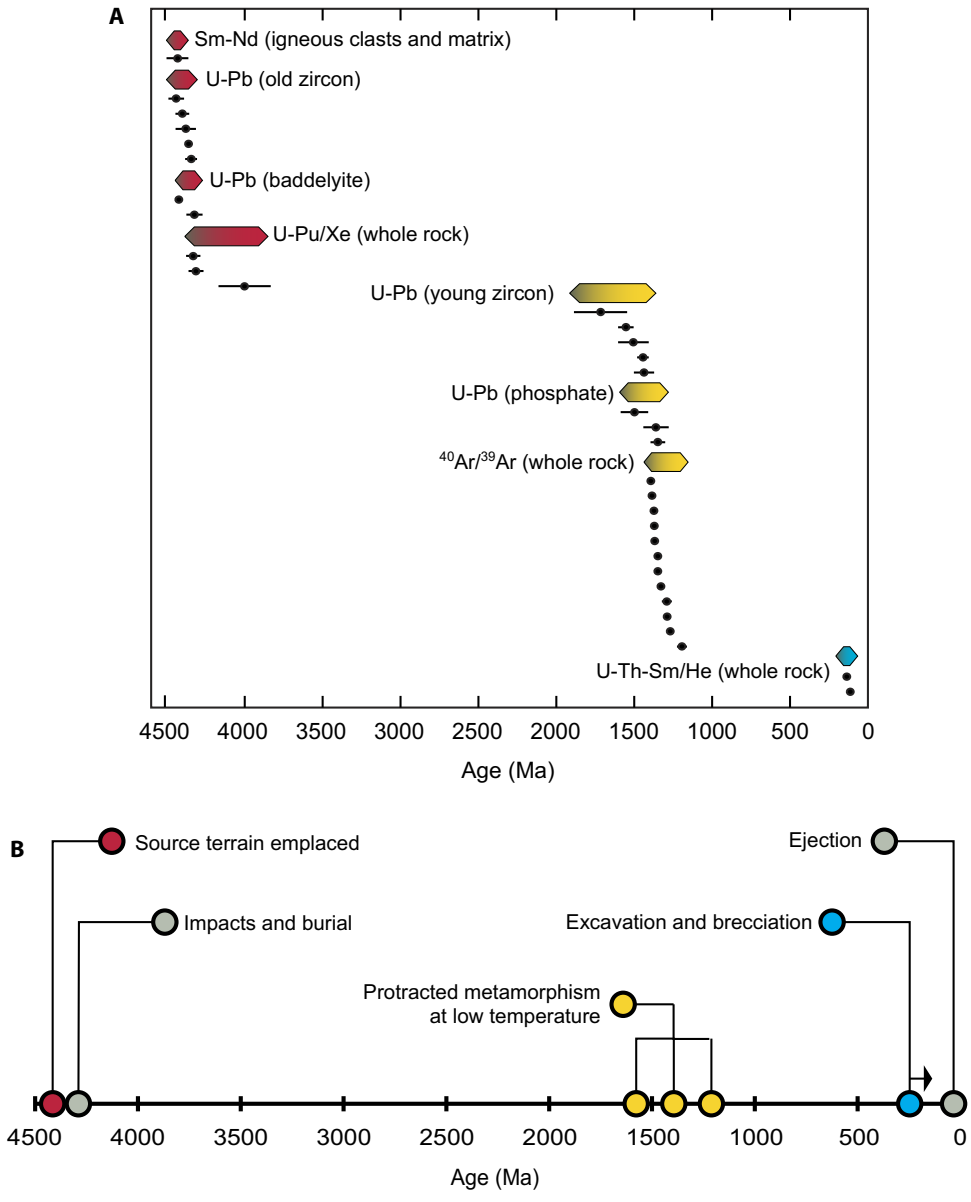

Fig. 1. Chronometric ages and the history of NWA 7034. (**A**) Summary of NWA 7034 radiometric ages. The horizontal widths of the boxes are defined by the maximum and minimum ages obtained from a given method plus or minus the associated 2σ uncertainties, respectively. U-Th-Sm/He, $^{40}Ar/^{39}Ar$, and U-Pu/Xe ages are from this study. U-Pb in phosphate ages are from the studies of McCubbin *et al.* (*6*), Yin *et al.* (*8*), and Bellucci *et al.* (*9*). U-Pb in young zircon ages are from the studies of McCubbin *et al.* (*6*), Tartèse *et al.* (*7*), and Yin *et al.* (*8*). U-Pb in old zircon ages are from the studies of Humayun *et al.* (*2*), McCubbin *et al.* (*6*), Tartèse *et al.* (*7*), and Yin *et al.* (*8*). U-Pb in baddelyite ages are from Tartèse *et al.* (*7*). Sm-Nd data are from Nyquist *et al.* (*5*). The whole-rock $^{40}Ar/^{39}Ar$ age from the study of Lindsay *et al.* (*11*) is included with the data from this study. $^{40}Ar/^{39}Ar$ ages from feldspars are not shown. (**B**) Chronology of major events in the history of NWA 7034 inferred from isotopic measurements (see main text for additional details). (i) The source lithology formed at 4420 ± 70 Ma. (ii) The source lithology was subject to impact events that created ancient impact melt rocks at ~4400 Ma. (iii) After almost 3000 Ma of quiescence, the terrain experienced several hundred million years of thermal metamorphism from 1500 to 1200 Ma. (iv) Following metamorphism, another ~1000 Ma of quiescence prevailed until brecciation at 225 Ma or later. (v) A final impact event after brecciation ejected NWA 7034 from the surface of Mars.

are from NWA 7034, whereas those analyzed at SUERC are from NWA 11522. A total of 4 feldspar mineral separates and 13 individual matrix/clast chips (weighing ~0.1 to 2.5 mg) from visibly monomict fragments were selected for $^{40}Ar/^{39}Ar$ measurements (fig. S1). He, Ne, Ar, Kr, and Xe isotopes were analyzed in larger, polymict whole-rock fragments (4 to 22 mg) in the Livermore Noble Gas Lab to calculate U-Th-Sm/He, U-Pu/Xe, and cosmic ray exposure (CRE) ages and to determine the isotopic composition of trapped noble gas components. Ar, Kr, and Xe data from three aliquots (LLNL-UI-1, LLNL-UI-2, and LLNL-UI-3) are from Cassata (*16*) (see Supplementary Materials). After noble gas extractions, the polymict whole-rock fragments were digested in mineral acids ($HF-HNO_3-HCl$) for major and trace element concentration measurements, which were performed at LLNL using a Thermo Scientific Element XR inductively coupled plasma mass spectrometer (ICP-MS). For U concentrations, samples were spiked with a high-purity ^{233}U spike and chemical purified from the bulk dissolutions. U-Th-Sm/He and U-Pu/Xe ages were calculated using the sample-specific chemical compositions determined by ICP-MS (see Supplementary

Materials). All measurements are reported with 2σ uncertainties, and all weighted averages are reported at the 95% confidence interval. Likewise, all uncertainties on previously reported data are listed at the 2σ level. Detailed descriptions of the analytical methods, data reduction procedures, and statistical treatment of results are provided in the Supplementary Materials.

RESULTS

$^{40}Ar/^{39}Ar$ chronometry

We conducted a total of 13 whole-rock fragment incremental heating experiments. Isochron diagrams and age spectra are shown in Figs. 2 and 3, respectively. Complete analytical results are given in the Supplementary Materials, and additional age spectra are shown in fig. S2. The whole-rock fragments generally yield plateaus over 50% or more of the total ^{39}Ar released from feldspathic phases within the whole-rock fragments, which yield low Ca/K ratios and degas at low temperatures in comparison to mafic phases. At low cumulative ^{39}Ar release fractions, age spectra are variably reset to subplateau ages by one or more younger thermal events (Fig. 3). Low-temperature discordance is generally confined to the first 15% of the cumulative gas released, although two fragments are extensively reset and did not yield plateaus (Fig. 3 and see also the Supplementary Materials). At high temperatures (high cumulative ^{39}Ar release fractions), step ages again decrease to subplateau values while the Ca/K ratio increases, before a monotonic increase in step ages occurs at the end of the heating experiments (Fig. 3). Such high-temperature discordance is common in meteoritic $^{40}Ar/^{39}Ar$ age spectra and is attributable to both recoil-implanted ^{39}Ar from a potassium (K)–rich donor phase (feldspar) into a K-poor receptor phase (pyroxene) [for example, the work of Huneke and Smith (*17*)] and to diffusive loss of ^{40}Ar from pyroxenes due to high-temperature shock heating (*18*, *19*). In the case of NWA 7034, ^{39}Ar recoil redistribution appears to be the cause of high-temperature discordance because matrix pyroxene and feldspar grain sizes (0.1 to 1 μm) (*1*) are comparable to the mean recoil length scale of ^{39}Ar (~0.1 μm) (*17*) and the rock is not significantly shocked (*4*). We excluded discordant low- and high-temperature extractions from isochron regressions and plateau age calculations discussed below (see the Supplementary Materials for a description of the statistical approach used to interpret age spectra and isochron diagrams).

Isochron ages were obtained from 7 of the 13 whole-rock fragments and range from 1367 ± 44 to 1224 ± 52 Ma (Fig. 2 and Table 1). The weighted average $^{40}Ar/^{36}Ar$ ratio of the trapped component inferred from these seven isochron regressions is 576 ± 208 [mean square weighted deviation (MSWD) = 8.8; Table 1]. Excess scatter in the isochron *y* intercepts likely reflects the inclusion of extractions that are deficient in ^{40}Ar or ^{39}Ar due to diffusive or recoil loss, respectively, which can result in isochron rotation while still providing statistically robust regressions. All age spectra were corrected for trapped ^{40}Ar using the weighted average trapped component inferred from the isochron regressions. The resulting plateau ages range from 1391 ± 16 to 1191 ± 32 Ma (Table 1). Most whole-rock fragments ($n = 7$ of 13) yielded ages between 1391 ± 16 and 1327 ± 12 Ma. The whole-rock $^{40}Ar/^{39}Ar$ results are generally slightly younger than U-Pb ages of phosphates and young zircons, which range from 1574 ± 38 to 1345 ± 47 Ma (*6*–*9*), and lower intercept U-Pb ages of old zircons, which range from 1712 ± 170 to 1434 ± 65 Ma (*2*, *7*, *8*).

We conducted a total of four feldspar incremental heating experiments. Representative age spectra are shown in Fig. 3. As with the whole-rock fragments, feldspar age spectra are variably reset by one or more thermal events occurring more recently than 1000 Ma, resulting in low-temperature discordance. One aliquot (SUERC-13) yielded concordant step ages, which define a weighted average of 1374 ± 7 Ma (MSWD = 7.2; Table 1). One aliquot (SUERC-14) is significantly disturbed due to diffusive loss, with maximum step ages of ~1500 Ma. Two aliquots (SUERC-12 and LLNL-3) yielded progressively older step ages with increasing temperature, with age maxima at >2000 Ma. The feldspar results are consistent with previous $^{40}Ar/^{39}Ar$ measurements of plagioclase and alkali feldspars, which yielded ages between 2250 ± 80 and 1285 ± 8 Ma (*11*, *12*), with one younger outlier at 788 ± 252 Ma (*12*). Feldspar ages that exceed 2000 Ma likely indicate that the thermal events responsible for resetting matrix and clast materials were insufficiently hot and/or protracted to completely reset larger feldspar mineral fragments.

U-Th-Sm/He chronometry

Two whole-rock fragments (LLNL-UI-4 and LLNL-UI-5) were analyzed for He isotopic abundances and then subsequently dissolved for U, Th, and Sm concentration measurements by ICP-MS. The samples yield U-Th-Sm/He ages of 135 ± 6 and 113 ± 4 Ma, with U concentrations of 0.73 ± 0.03 and 0.83 ± 0.02 parts per million (ppm), respectively (Supplementary Materials). Cartwright *et al.* (*10*) measured a similar concentration of ^{4}He but calculated a slightly older U-Th/He age of 170 Ma, assuming a U concentration of 0.51 ppm as determined by Agee *et al.* (*20*) on a different whole-rock fragment. The individual U-Th-Sm/He ages do not agree within analytical uncertainties, likely because of incomplete degassing of ^{4}He from the polymineralic aliquots during brecciation, ejection, and/or other metamorphic events (discussed in detail below).

U-Pu/Xe chronometry

Three whole-rock fragments (LLNL-UI-1, LLNL-UI-2, and LLNL-UI-3) were analyzed for Xe isotopic abundances and then subsequently dissolved for U and Nd concentration measurements by ICP-MS. The total abundance of fission Xe in each aliquot exceeds that which could have been produced by spontaneous fission of ^{238}U since 4400 Ma. For example, apparent U-Xe ages are 9111 ± 813, 4541 ± 636, and 11944 ± 1002 Ma (Table 2), based on U concentration measurements of 0.44 ± 0.02, 0.43 ± 0.02, and 0.166 ± 0.002 ppm, respectively (Supplementary Materials). Collectively, these observations indicate that the source lithologies formed while ^{244}Pu was live ($t_{1/2}$ = 81.8 Ma). U-Pu/Xe ages can be calculated using the Solar System initial ratio of either $^{244}Pu/U$ or $^{244}Pu/Nd$. Assuming a Solar System initial $^{244}Pu/U$ ratio of 0.0068 ± 0.010 (*21*), apparent U-Pu/Xe ages are 4274 ± 44, 3963 ± 126, and 4358 ± 47 Ma (Table 2). Cartwright *et al.* (*10*) measured a slightly lower U-Pu/Xe age of 3880 +90, −160 Ma, assuming a U concentration of 0.51 ppm as determined by Agee *et al.* (*20*) on a different whole-rock fragment and chondritic $^{244}Pu/U$. Assuming a Solar System initial $^{244}Pu/Nd$ ratio of 0.00015 (*22*), with an arbitrarily assigned 15% uncertainty, and based on Nd concentration measurements of 16.7 ± 0.7, 13.8 ± 0.3, and 15.1 ± 0.9 ppm (Supplementary Materials), apparent U-Pu/Xe ages are 4319 ± 46, 3990 ± 167, and 4301 ± 48 Ma, respectively (Table 2). These ages are comparable to the Sm-Nd age of the source terrain (4420 ± 70 Ma) (*5*) and old U-Pb ages obtained from baddeleyite and zircon, which range from 4428 ± 50 to 4311 ± 52 Ma (*2*, *6*–*8*). Given the geochemical coherence of Pu and Nd (*23*), the U-Pu/Xe ages calculated on the basis of the Solar System initial $^{244}Pu/Nd$ are used throughout the remainder of the paper for discussion.

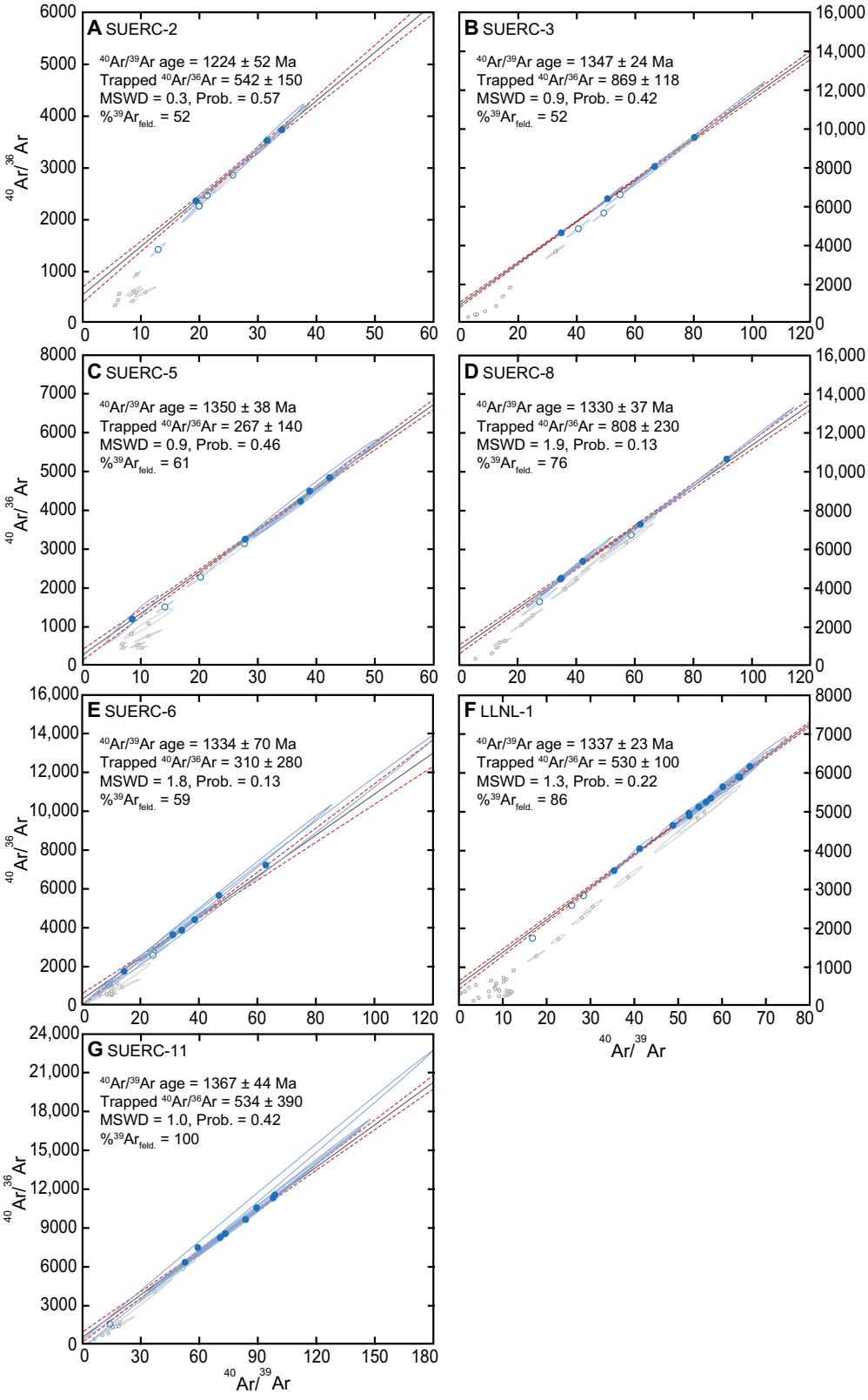

Fig. 2. $^{40}Ar/^{39}Ar$ isochron diagrams. Data shown in blue are derived from relatively K-rich (felsic) phases. Filled symbols were included in isochron regressions (see the Supplementary Materials for details regarding isochron regressions). Data shown in gray are derived from relatively K-poor phases that appear to be affected by ^{39}Ar recoil and were excluded from isochron regressions. Error ellipses reflect the uncertainty correlation and ±2σ analytical uncertainties. The confidence intervals on the isochron regressions (red lines) are shown at 2 SE.

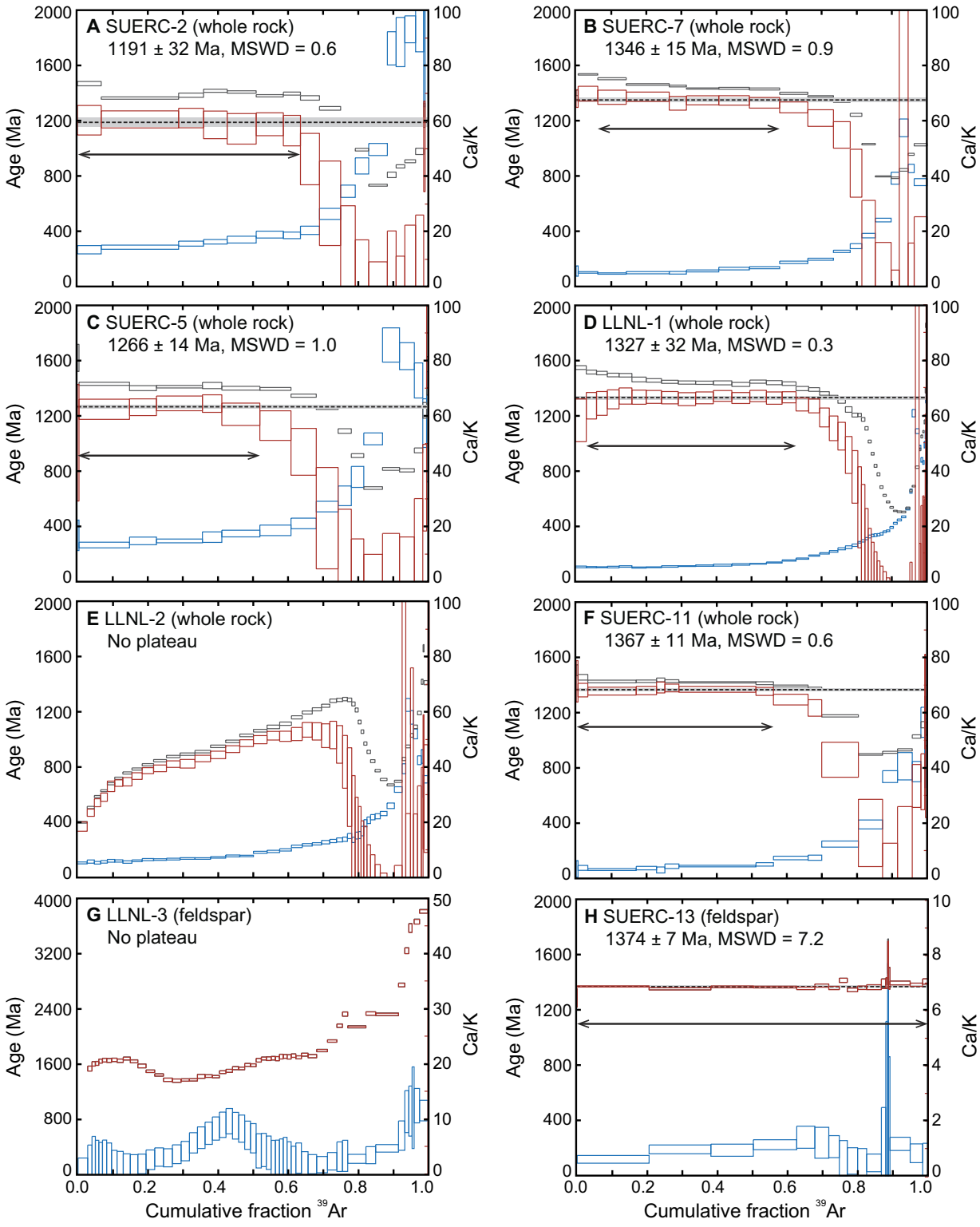

Fig. 3. ^{40}Ar/^{39}Ar age spectra. Age and Ca/K spectra obtained from whole-rock fragments and feldspar separates. ^{40}Ar/^{39}Ar ages are shown without and with martian atmospheric corrections as gray and red boxes, respectively, and are plotted against the primary *y* axis. Ca/K spectra are shown in blue and are plotted against the secondary *y* axis. Each spectrum is plotted against the cumulative release fraction of ^{39}Ar released. Vertical dimensions of the boxes reflect the ±2σ analytical uncertainties. The horizontal dashed black lines and associated gray bands reflect the plateau ages and their associated 2 SE uncertainties, respectively. Horizontal arrows denote steps that were included in plateau ages (see the Supplementary Materials for details regarding plateau calculations).

Table 1. $^{40}Ar/^{39}Ar$ results. $\%^{39}Ar_{feld}$ is the cumulative percentage of ^{39}Ar released from the feldspathic portion of the age spectrum that is included in the age calculation. The preferred age for each sample is the plateau age, shown in bold. Data were corrected for cosmogenic Ar using an apparent ^{38}Ar exposure age of 4.77 ± 0.54 Ma (see Table 3). Age spectra were corrected for trapped ^{40}Ar using a $^{40}Ar/^{36}Ar$ ratio of 576 ± 208, based on the weighted average *y* intercept of seven isochrons. See the Supplementary Materials for a list of extractions included in isochron regressions and plateau age calculations and for a description of the statistical approach used to interpret age spectra and isochrons and to calculate weighted averages.

		Isochron analysis					Age spectrum analysis		
Aliquot	**Phase**	**Age ± 2σ (Ma)**	**$(^{40}Ar/^{36}Ar)_{trap}$ ± 2σ**	**MSWD**	**Prob.**	**$\%^{39}Ar_{feld}$**	**Age ± 2σ (Ma)**	**MSWD**	**$\%^{39}Ar_{feld}$**
SUERC-1	WR frag		Does not meet isochron criteria				<1300 Ma—did not yield concordant ages		
SUERC-2	WR frag	1224 ± 52	542 ± 150	0.3	0.57	52	**1191 ± 32**	0.6	92
SUERC-3	WR frag	1347 ± 24	869 ± 118	0.9	0.42	52	**1391 ± 16**	0.8	52
SUERC-4	WR frag		No spread on isochron				**1365 ± 16**	0.7	64
SUERC-5	WR frag	1350 ± 38	267 ± 140	0.9	0.46	61	**1266 ± 14**	1.0	76
SUERC-6	WR frag	1334 ± 70	310 ± 280	1.8	0.13	59	**1288 ± 32**	1.2	59
SUERC-7	WR frag		Does not meet isochron criteria				**1346 ± 15**	0.9	89
SUERC-8	WR frag	1330 ± 37	808 ± 230	1.9	0.13	76	**1371 ± 16**	0.7	76
SUERC-9	WR frag		Does not meet isochron criteria				**1345 ± 17**	1.3	69
SUERC-10	WR frag		No spread on isochron				**1383 ± 16**	1.8	56
SUERC-11	WR frag	1367 ± 44	534 ± 390	1.0	0.42	100	**1367 ± 11**	0.6	100
LLNL-1	WR frag	1337 ± 23	530 ± 100	1.3	0.22	86	**1327 ± 12**	0.3	95
LLNL-2	WR frag		Does not meet isochron criteria				<1300 Ma—did not yield concordant ages		
		Weighted average:	**576 ± 208**	**8.8**					
SUERC-12	Feldspar		Does not meet isochron criteria				>2000 Ma—did not yield concordant ages		
SUERC-13	Feldspar		Does not meet isochron criteria				**1374 ± 7***	7.2	100
SUERC-14	Feldspar		Does not meet isochron criteria				>1400 Ma—did not yield concordant ages		
LLNL-3	Feldspar		Does not meet isochron criteria				>2000 Ma—did not yield concordant ages		

*The SUERC-13 feldspar age represents the weighted average of all extraction steps and does not satisfy plateau age criteria.

Table 2. U-Pu/Xe ages. Age uncertainties include uncertainties on [Nd], [U], [^{136}Xe], Solar System initial Pu/U and Pu/Nd ratios, ^{136}Xe cumulative yields, branching ratios, and ^{238}U and ^{244}Pu decay constants.

	No Pu	Pu/U* assumed	Pu/Nd† assumed
Aliquot	**Age ± 2σ (Ma)**	**Age ± 2σ (Ma)**	**Age ± 2σ (Ma)**
LLNL-UI-1	9111 ± 813	4274 ± 44	4319 ± 46
LLNL-UI-2	4541 ± 636	3963 ± 126	3990 ± 167
LLNL-UI-3	11944 ± 1002	4358 ± 47	4301 ± 48

*On the basis of a Solar System initial Pu/U = 0.0068 ± 0.0010 [Hudson *et al.* (*21*)]. †On the basis of a Solar System initial Pu/Nd = 0.00015 [Lugmair and Marti (*22*)]. No uncertainty is given in Lugmair and Marti (*22*). A 15% uncertainty is assumed here.

Cosmogenic nuclides

Apparent ^{3}He, ^{21}Ne, ^{38}Ar, ^{78}Kr, and ^{83}Kr CRE ages, calculated on the basis of the whole-rock composition determined by ICP-MS (Supplementary Materials) and element-specific galactic cosmic ray (GCR) production rates at a nominal shielding of 40 g/cm^2 (*24*), are listed in Table 3. The cosmogenic nuclides yield weighted average exposure ages of 2.14 ± 0.25 Ma (MSWD = 1.96), 4.11 ± 0.49 Ma (MSWD = 23.4), 4.77 ± 0.54 Ma (MSWD = 2.63), 12.1 ± 1.7 Ma (MSWD = 1.13), and 8.7 ± 1.6 Ma (MSWD = 0.23), respectively. Cartwright *et al.* (*10*) obtained apparent ^{3}He, ^{21}Ne, and ^{38}Ar exposure ages of 5.1, 11.4, and 5.4 Ma, respectively, at nominal shielding. Although there is agreement between ^{38}Ar exposure ages for our work and Cartwright *et al.* (*10*), ^{3}He and ^{21}Ne exposure ages differ considerably between the two studies. The source of the discrepancies is unclear but may be related to variations in the chemical composition used to calculate exposure ages. The exposure ages reported here represent the average of replicate analyses (Table 3) and are therefore unlikely to be biased by sample-to-sample variations in chemical composition. The differences in apparent ^{3}He, ^{21}Ne, ^{38}Ar, ^{78}Kr, and ^{83}Kr exposure ages indicate that (i) shielding differed considerably from "nominal" (40 g/cm^2), (ii) a complex irradiation history involving pre-ejection irradiation or in-transit breakup occurred, (iii) some cosmogenic nuclides were lost due to heating during ejection from Mars, if pre-exposure occurred, or during terrestrial atmospheric entry, and/or (iv) solar cosmic ray (SCR)

Table 3. Apparent CRE ages at nominal shielding. All production rates were calculated using the equations of Eugster and Michel (*24*) for a nominal shielding of 40 g/cm^2, with P21 modified to account for Na using the Na/Mg production rate at 40 g/cm^2 of shielding from Hohenberg *et al.* (*61*). All production rates are based on the whole-rock composition determined by ICP-MS (see the Supplementary Materials), with SiO_2 from Agee *et al.* (*20*). The weighted average ages, including production rate uncertainties, are shown in bold.

	^{3}He*	^{21}Ne†	^{38}Ar‡	^{78}Kr§	^{83}Kr¶
Aliquot	**CRE age ± 2σ (Ma)**	**CRE age ± 2σ (Ma)**	**CRE age ± 2σ (Ma)**	**CRE age ± 2σ (Ma)**	**CRE age ± 2σ (Ma)**
LLNL-UI-1	— ± —	4.05 ± 0.08	4.63 ± 0.16	12.26 ± 3.62	9.12 ± 3.04
LLNL-UI-2	— ± —	4.1 ± 0.08	4.76 ± 0.28	11.22 ± 1.72	8.27 ± 1.92
LLNL-UI-3	— ± —	4.05 ± 0.06	5.16 ± 0.3	13.24 ± 2.08	9.2 ± 2.36
LLNL-UI-4	2.46 ± 0.48	5.18 ± 0.24	5.09 ± 0.8	— ± —	— ± —
LLNL-UI-5	2.11 ± 0.14	4.42 ± 0.22	4.8 ± 0.26	— ± —	— ± —
Weighted average‖	2.14 ± 0.13	4.11 ± 0.26	4.77 ± 0.25	12.07 ± 1.24	8.73 ± 1.34
MSWD	1.96	23.43	2.63	1.13	0.23
CRE age w/ PR unc.**	**2.14 ± 0.25**	**4.11 ± 0.49**	**4.77 ± 0.54**	**12.07 ± 1.73**	**8.73 ± 1.6**

*Calculated using P3 = 7.54 × 10^{-13} mol/g per million years. †Calculated based on total ^{21}Ne, using P21 = 1.06 × 10^{-13} mol/g per million years. ‡Calculated assuming the trapped ^{38}Ar/^{36}Ar ratio is 0.189, using P38 = 4.78 × 10^{-15} mol/g per million years. §Calculated using P78 = 1.12 × 10^{-17} mol/g per million years. ¶Calculated using P83 = 7.36 × 10^{-17} mol/g per million years. ‖See the Supplementary Materials for details on weighted average calculations.
**Systematic uncertainties on cosmogenic nuclide production rates (PR unc.) are assumed to be 10%.

contributions are significant. These irradiation scenarios are explored in more detail below.

DISCUSSION

Igneous age of the source lithology

The bimodal distribution of U-Pb ages obtained from zircon, baddelyite, and phosphates (4400 to 4300 Ma and 1700 to 1300 Ma) could reflect either multiple source lithologies or selective resetting associated with secondary thermal events (*5*). On the basis of a 4420 ± 70 Ma Sm-Nd isochron age obtained from both matrix and clast mineral separates, which is indistinguishable from the old population of zircon and baddelyite ages, Nyquist *et al.* (*5*) concluded that the various lithological components formed contemporaneously and the source terrain is ancient. The U-Pu/Xe ages obtained from whole-rock fragments (4319 ± 46, 3990 ± 167, and 4301 ± 48 Ma; Table 2) confirm this finding.

Re-Os data indicate that the terrain was subject to impacts early in its history, at ~4400 Ma (*25*), which presumably created the impact melt clasts within the breccia (*4*). These impact melt rocks are likely the host of retentively held ancient atmospheric gases (*16*) that were incorporated in high concentrations via shock implantation (*26*). Following emplacement near the martian surface and subsequent impact processing, the terrain experienced a period of quiescence during which no metamorphic events are recorded by the U-Pb system in zircon (*6*). It is possible that the terrain was buried by volcanic processes or the deposition of sediments or impact ejecta, apparently shielding it from impact metamorphism and redistribution.

Contact metamorphism between 1500 and 1200 Ma

After almost 3000 Ma of quiescence, the terrain experienced several hundred million years of thermal metamorphism recorded by the K-Ar and U-Pb systems. ^{40}Ar/^{39}Ar measurements of whole-rock fragments yield plateau ages that range from 1391 ± 16 to 1191 ± 32 Ma (Table 1), slightly younger than the range in U-Pb ages of phosphates and young zircons (*2*, *6*–*9*). The age differences exceed measurement uncertainties and are greater than durations (10's of Ma or less) required to cool shock-heated basement terrains following large (100 to 200 km) impact events that might have occurred at ~1300 Ma (*27*). These observations suggest that the K-Ar system in igneous clasts and matrix minerals and the U-Pb system in phosphates were reset by a protracted series of metamorphic events that varied spatially and temporally across the source terrain. Discordances observed in the Rb-Sr system (*5*) and partial resetting of the Re-Os system (*25*) are likely due to these metamorphic events. The metamorphic conditions were insufficient to completely reset the K-Ar system in millimeter-sized feldspar mineral fragments or to degas ancient atmospheric noble gases that appear to be hosted in retentive clasts or larger phenocrysts that degas at high laboratory heating temperatures (*16*). Selective resetting of chronometers is most easily accomplished at low temperatures, where differences in diffusivity are generally more pronounced.

The ancient U-Pu/Xe ages further demonstrate that these secondary thermal events did not significantly alter the distributions of U or Nd or cause significant diffusive loss of Xe. It thus appears that the U-Pb system in phosphates is more readily reset than the U-Pu/Xe system in NWA 7034. Closure temperatures for Pb diffusion in 1- to 10-μm domains of gem-quality fluorapatite (Durango, Mexico) range from 347 to 414°C (for spherical geometry and a 10°C/Ma cooling rate), with an activation energy of 231 kJ/mol (*28*). The applicability of such diffusion parameters to radiation-damaged chlorapatites like those in NWA 7034 is unclear. Data on the diffusion of Xe in silicates are sparse, but generally indicate a high activation energy for diffusion (>300 kJ/mol) (*15*, *29*). Such strong temperature dependence for Xe diffusion may result in a lower diffusivity than Pb if secondary thermal events occurred at low temperatures. Regardless, the ancient U-Pu/Xe ages suggest that (i) any subsequent thermal events were insufficiently hot and/or protracted to mobilize Xe and (ii) aqueous alteration and breccia formation did not introduce a significant proportion of U-bearing minerals.

Plume-related magmatism in the NWA 7034 source terrain may have promoted low-temperature metamorphism over a 300-Ma period, possibly through the intrusion of large dike and sill or plutonic complexes. Martian plume–fed edifices have remained connected to their magma sources, at least in some instances, for billions of years (*30*). Crater density distributions indicate that several martian volcanic centers were active for hundreds of millions of years at 2000 to 1000 Ma (*31*), and measurements of nakhlite age variations provide direct evidence for a volcanic center that formed over at least 93 ± 12 Ma during this time period (*32*). Magmatic intrusions associated with the volcanic center likely drove hydrothermal systems that produced secondary alteration phases such as overgrowths observed at phosphate grain margins (*3*). Most whole-rock fragments ($n = 7$ of 13) yielded ages between 1391 ± 16 and 1327 ± 12 Ma (Table 1), suggesting that plume-related activity in the NWA 7034 source terrain may have peaked at ~1350 Ma.

Brecciation at 225 Ma or later

Following metamorphism, >1000 Ma of quiescence appears to have prevailed until another event occurred, as recorded by U-Th-Sm/He ages of 135 ± 6 and 113 ± 4 Ma. Two end-member explanations for these ages merit consideration. First, it is possible that the U-Th-Sm/He system was nearly completely reset by a low-temperature thermal event such as impact-related brecciation that occurred at ~110 Ma. Second, it is possible that the U-Th-Sm/He system was partially reset from 1500–1200 Ma to 135–113 Ma during ejection. We consider the latter scenario unlikely because NWA 7034 is only shocked to 5 to 15 GPa (*4*), near the theoretical minimum associated with the acceleration of surface rocks beyond the planetary escape velocity (*33*). U-Th/He measurements of martian meteorites have demonstrated that He loss during ejection scales with peak shock pressure (*34*, *35*). Nakhlites that have been shocked to <20 GPa (*36*) yield U-Th/He ages that overlap $^{40}Ar/^{39}Ar$ ages to within 50% (*35*). These observations are consistent with theoretical predictions of postshock temperatures associated with shock pressures of 5 to 15 GPa, which do not exceed 20°C (*36*). Because NWA 7034 was shocked at even lower pressures than the nakhlites, it appears unlikely that significant heating and diffusive loss of ^{4}He occurred during ejection. We thus suggest that the U-Th-Sm/He ages constrain brecciation to have occurred no earlier than 225 Ma, based on an upper limit of ~50% loss of ^{4}He during ejection and the youngest U-Th-Sm/He age (113 ± 2 Ma).

Additional evidence for brecciation at 225 Ma or later is provided by $^{40}Ar/^{39}Ar$ age spectra, which yield subplateau ages during low-temperature extractions, with age minima at ~400 to 200 Ma (Fig. 3 and Supplementary Materials). Similarly, U-Pb concordia diagrams indicate that one or more disturbances postdate 1500 to 1200 Ma, with lower intercept ages of 0 ± 100, 209 ± 850, and 392 ± 540 Ma (*6*–*8*). Finally, brecciation at 225 Ma or later provides an explanation for the K-feldspar $^{40}Ar/^{39}Ar$ isochron age of 788 ± 252 Ma reported by Lindsay *et al.* (*12*), which presumably reflects detrital material that was incorporated during brecciation (*12*).

It is also possible that the NWA 7034 source breccia formed during the flank collapse of a large shield volcano, which could provide a mechanism to mix material that was heated by a volcanic center over a 300-Ma duration. Because flank collapse is not a priori associated with heating, if the breccia formed at this time, then the ambient temperature at the depth from which the rocks were exhumed must have been sufficiently hot to preclude quantitative retention of ^{4}He and to cause the minor disturbances to the K-Ar and U-Pb systems noted above.

CRE history

As noted above, there are large discrepancies in apparent CRE ages calculated using production rates for nominal shielding (Table 3). NWA 7034 contains ^{80}Kr and ^{82}Kr produced by neutron capture on ^{79}Br and ^{81}Br, respectively (*10*, *16*). The production of measureable abundances of these neutron capture nuclides requires the NWA 7034 meteoroid to be of sufficient size to slow secondary neutrons to epithermal or thermal energies. Cartwright *et al.* (*10*) suggested that the NWA 7034 was irradiated in the center of a >50-cm meteoroid, in which the predicted $^{22}Ne/^{21}Ne$ ratio based on the model of Leya and Masarik (*37*) is consistent with their measurement and shielding is sufficient to slow secondary neutrons to thermal energies. Irradiation at depth, however, did not reconcile apparent differences between ^{3}He, ^{21}Ne, and ^{38}Ar exposure ages (*10*). Because we obtained different ^{3}He and ^{21}Ne exposure ages than Cartwright *et al.* (*10*), we explored solutions to the problem that involved more shielding and contributions from SCRs. We used depth-dependent GCR production rates (*37*), extended to small meteoroids, to model the exposure history. In addition, SCR production was calculated using the model of Trappitsch *et al.* (*38*). In both cases, we determined elementary production rates using the whole-rock composition obtained by ICP-MS (Supplementary Materials). Although the stopping and secondary particle spectra used to calculate these production rates are based on ordinary chondrites, we did not expect them to vary by more than approximately 20% because of difference in meteoroid chemistry (*39*). We varied meteoroid size and depth of irradiation to find exposure histories that best reproduced the measured $^{21}Ne/^{22}Ne$ ratio of aliquot LLNL-UI-5 (0.799 ± 0.018; Supplementary Materials) and minimized the relative SD between the ^{3}He, ^{21}Ne, and ^{38}Ar exposure ages (Table 3).

The measured $^{21}Ne/^{22}Ne$ ratio in NWA 7034 is at the lower limit of the range observed in stony meteorites (*24*). Combined GCR and SCR irradiation, as has been observed in some shergottites and ordinary chondrites with small recovery masses (*39*, *40*), could explain the disparate results obtained from ^{3}He, ^{21}Ne, ^{22}Ne, and ^{38}Ar. However, NWA 7034 would be required to come from the surface of a sufficiently large meteoroid such that it is irradiated by SCRs on the surface and receives secondary neutrons at epithermal or thermal energies from the back side to produce ^{80}Kr and ^{82}Kr by neutron capture on ^{79}Br and ^{81}Br, respectively. This is problematic because most large meteorites do not preserve their SCR record because of ablation during passage through Earth's atmosphere (*41*). If solely GCR production is considered, then an irradiation location in either a small meteoroid (<10 cm) or at depth in a larger meteoroid (>50 cm) can reproduce the measured $^{21}Ne/^{22}Ne$ ratio (fig. S3) (*10*). However, irradiation in a small meteoroid does not yield concordant CRE ages. For example, a shielding depth of 6.6 to 6.8 cm in a meteoroid with a radius of 7 cm reproduces the $^{21}Ne/^{22}Ne$ ratio, but the resulting CRE ages are 2.55 ± 0.26, 4.82 ± 0.48, and 6.58 ± 0.66 Ma for ^{3}He, ^{21}Ne, and ^{38}Ar, respectively, assuming a 10% uncertainty on production rates. Irradiation at the center of a meteoroid with radius >120 cm reproduces the $^{21}Ne/^{22}Ne$ ratio and yields CRE ages with a relative SD of ~10% or less, comparable to the uncertainties on GCR production rates. For example, the best-fit irradiation history is at a depth of 280 to 284 cm in a meteoroid with a radius of 300 cm, which yields $^{21}Ne/^{22}Ne$ = 0.792 Ma and ^{3}He, ^{21}Ne, and ^{38}Ar exposure ages of 263 ± 26, 252 ± 25, and 256 ± 26 Ma, respectively. Such an extended transit duration is inconsistent with that of other martian meteorites and is older than the U-Th-Sm/He ages of 135 ± 6 and 113 ± 4 Ma but could reflect pre-ejection irradiation after brecciation, followed

by in-transit irradiation for ~1 to 2 Ma. Alternatively, reasonable fits to the data are obtained at a depth of 114 to 116 cm in a meteoroid with a radius of 120 cm, which yields $^{21}Ne/^{22}Ne$ = 0.798 Ma and ^{3}He, ^{21}Ne, and ^{38}Ar exposure ages of 7.7 ± 0.8, 8.9 ± 0.9, and 9.6 ± 1.0 Ma, respectively. Unfortunately, it is not possible to uniquely solve for the ejection age, but it is clear that much of the irradiation occurred under significant shielding (*10*) and the ejection event likely occurred earlier than the ~5 Ma that would be inferred from the ^{21}Ne and ^{38}Ar exposure ages at nominal shielding.

Implications for the age of the martian crustal dichotomy

The martian crustal dichotomy, a topographic and geophysical divide between the heavily cratered southern highlands and smoother plains of the northern lowlands, is thought to have formed by either an exogenous (impact-related) or endogenous (mantle-related) origin (*42*). Exogenous hypotheses involve a giant impact in either the northern hemisphere (*43*, *44*) or the southern hemisphere (*45*–*48*). In southern hemisphere impact scenarios, the highlands are formed after the giant impact, due to melt formation and ascent in the impact region [a hemispherical magma ocean; (*45*)]. In northern hemisphere impact scenarios, rocks in the southern highlands predate the giant impact and are covered in up to 25 km of ejecta from the giant impact (*49*). Empirical evidence for such a giant impact event might be found in Mars' elevated highly siderophile element abundances, which, if caused by exogenous material delivered after core formation and silicate differentiation, would likely require an impact with a Ceres-sized planetesimal (*50*). Endogenous hypotheses generally involve degree-1 mantle convection (that is, planetary-scale convection) with upwelling directed beneath either the southern or the northern hemisphere (*49*, *51*–*53*). In northern hemisphere scenarios, upwelling thins and erodes the overlying crust, which is then accreted in the southern hemisphere (*53*). In southern hemisphere scenarios, upwelling promotes extensive melting and the formation of a thicker crust above the plume (*51*, *54*). Alternatively, overturn of an unstable mantle following crystallization of an early magma ocean may have thickened the crust (*55*). Estimates for the age of the dichotomy from geophysical models range from ~4500 Ma (*52*) to several hundred million years after planetary formation (*54*), depending on parameters such as mantle viscosity and the inferred mechanism promoting crustal thickening (for example, mantle overturn or a layered viscosity structure).

Chronometric data obtained from NWA 7034 place constraints on near-surface processing and metamorphism in the martian crust over the past 4420 ± 70 Ma and, therefore, may shed light on the age of the crustal dichotomy and its formation mechanism. In particular, $^{40}Ar/^{39}Ar$, U-Th-Sm/He, and Sm-Nd measurements indicate that regional terrains with areal extents of at least hundreds of square kilometers likely remained near the martian surface in the southern hemisphere since 4400 Ma. These observations may limit the timing of putative giant impacts and crustal growth associated with southern hemisphere upwelling in degree-1 convection hypotheses, and thus may constrain the time at which the martian crustal dichotomy formed.

The observation of U-Pb and $^{40}Ar/^{39}Ar$ metamorphic ages that span 1500 to 1200 Ma indicates that heating of the NWA 7034 source terrain varied spatially and temporally over a 300-Ma period. Plume-related magmatism likely drove crustal heating because the time scales associated with impact heating are too short to plausibly explain such an observation. The areal extents of large volcanic centers associated with plume-driven magmatism are thousands of square kilometers (*30*) and reasonably constrain the maximum size of the source terrain. Ubiquitous resetting of the K-Ar system in matrix minerals and the U-Pb system in phosphates suggests that crustal heating was not localized on the kilometer scale [for example, because of the intrusion of small (meter scale) dikes and sills] and, thus, reasonably constrains the minimum size of the source terrain to be greater than tens of square kilometers.

Brecciation did not occur until 225 Ma or later (as constrained by U-Th-Sm/He measurements), which indicates that any cratering event that excavated the source terrain was likely less than 50 to 60 km in size, the largest events that occurred at that time (*56*). This in turn suggests that the source terrain remained within ~3 to 4 km of the martian surface since formation at 4420 ± 70 Ma, as deeper depths of burial would preclude excavation. Alternatively, the source terrain may have been shielded near or above the surface by a comparatively young volcanic complex until brought to the surface by a flank collapse. Depths of burial shallower than a few hundred meters are also likely precluded because it is statistically implausible that smaller impactors generating craters up to a few kilometers in diameter would not have hit the source terrain throughout its 4400-Ma history [that is, the martian surface is saturated by such craters (*56*)].

Although it is difficult to determine where the NWA 7034 source terrain was emplaced, the following observations suggest that it was the southern highlands. First, the matrix and impact melt clast major element compositions and the bulk-rock infrared absorption spectrum are consistent with rocks currently found in the southern highlands (*2*, *6*, *20*, *57*). Second, ancient terrains in the northern lowlands are, in many locations, buried in >5 km of overlying sediment and volcanic units (*58*) and are therefore less likely to have been excavated by impact events at 225 Ma or later. Finally, most active volcanism at 1500 to 1200 Ma is focused in the southern highlands and near the Tharsis and Elysium regions, with the Tharsis volcanoes remaining active throughout much of martian history (*30*).

Collectively, data from NWA 7034 and paired stones thus indicate that cohesive volcanic terrains have likely survived within a few kilometers of the martian surface, at least in one locality ostensibly in the southern hemisphere, since >4400 Ma. It follows from this conclusion that if the dichotomy formed because of a giant impact, it is unlikely to have postdated the formation of the NWA 7034 source lithology at 4420 ± 70 Ma. Depending on whether the southern or northern hemisphere was struck, the putative giant impact would have melted or deeply buried near-surface terrains in the southern hemisphere, respectively. Regarding endogenic hypotheses, the near-surface history of NWA 7034 suggests that crustal growth associated with a southern hemisphere upwelling occurred within ~100 to 200 Ma of planet formation. Longer crustal growth durations spanning 500 to 1000 Ma [for example, select models in Keller and Tackley (*51*) and Šrámek and Zhong (*54*)] are more likely to have buried near-surface terrains. For example, assuming an intrusive-to-extrusive volcanic ratio of 8.5 to 10 (*25*) and average crustal thickness in the cratered highlands of 59 km (*59*), 5 to 7 km of volcanic deposits are predicted to have formed during crustal production, consistent with observations of layered volcanic/sedimentary rocks in Valles Marineris (8 km) (*60*). The NWA 7034 source terrain is therefore unlikely to have remained within 3 to 4 km of the martian surface, unless it formed near the end of crustal production. Thus, for giant impact and southern hemisphere upwelling scenarios, data from NWA 7034 suggest that formation of the martian crustal dichotomy predates 4420 ± 70 Ma. Data from NWA 7034 cannot be used to constrain the age of the dichotomy if crustal growth is associated with northern hemisphere upwelling due to degree-1 convection,

because southern hemisphere crustal growth via this mechanism is driven largely by lithospheric accretion (*53*).

SUPPLEMENTARY MATERIALS

Supplementary material for this article is available at http://advances.sciencemag.org/cgi/content/full/4/5/eaap8306/DC1
Supplementary Materials and Methods
fig. S1. Image of NWA 11522.
fig. S2. $^{40}Ar/^{39}Ar$ age spectra.
fig. S3. Irradiation modeling of NWA 7034.
data file S1. Complete analytical data set (Excel file).
References (*62*–*82*)

REFERENCES AND NOTES

1. A. R. Santos, C. B. Agee, F. M. McCubbin, C. K. Shearer, P. V. Burger, R. Tartèse, M. Anand, Petrology of igneous clasts in Northwest Africa 7034: Implications for the petrologic diversity of the martian crust. *Geochim. Cosmochim. Acta* **157**, 56–85 (2015).
2. M. Humayun, A. Nemchin, B. Zanda, R. H. Hewins, M. Grange, A. Kennedy, J.-P. Lorand, C. Göpel, C. Fieni, S. Pont, D. Deldicque, Origin and age of the earliest Martian crust from meteorite NWA 7533. *Nature* **503**, 513–516 (2013).
3. Y. Liu, C. Ma, J. R. Beckett, Y. Chen, Y. Guan, Rare-earth-element minerals in martian breccia meteorites NWA 7034 and 7533: Implications for fluid–rock interaction in the martian crust. *Earth Planet. Sci. Lett.* **451**, 251–262 (2016).
4. A. Wittmann, R. L. Korotev, B. L. Jolliff, A. J. Irving, D. E. Moser, I. Barker, D. Rumble III, Petrography and composition of Martian regolith breccia meteorite Northwest Africa 7475. *Meteorit. Planet. Sci.* **50**, 326–352 (2015).
5. L. E. Nyquist, C.-Y. Shih, F. M. McCubbin, A. R. Santos, C. K. Shearer, Z. X. Peng, P. V. Burger, C. B. Agee, Rb-Sr and Sm-Nd isotopic and REE studies of igneous components in the bulk matrix domain of Martian breccia Northwest Africa 7034. *Meteorit. Planet. Sci.* **51**, 483–498 (2016).
6. F. M. McCubbin, J. W. Boyce, T. Novák-Szabó, A. R. Santos, R. Tartèse, N. Muttik, G. Domokos, J. Vazquez, L. P. Keller, D. E. Moser, D. J. Jerolmack, C. K. Shearer, A. Steele, S. M. Elardo, Z. Rahman, M. Anand, T. Delhaye, C. B. Agee, Geologic history of Martian regolith breccia Northwest Africa 7034: Evidence for hydrothermal activity and lithologic diversity in the Martian crust. *J. Geophys. Res. Planets* **121**, 2120–2149 (2016).
7. R. Tartèse, M. Anand, F. M. McCubbin, A. R. Santos, T. Delhaye, Zircons in Northwest Africa 7034: Recorders of crustal evolution on Mars, in *45th Lunar and Planetary Science Conference*, The Woodlands, Texas, 17 to 21 March 2014 (LPSC 2014), Abstract # 2020.
8. Q. Z. Yin , F. M. McCubbin, Q. Zhou, A. R. Santos, R. Tartèse, X. Li, Q. Li, Y. Liu, G. Tang, J. W. Boyce, Y. Lin, W. Yang, J. Zhang, J. Hao, S. M. Elardo, C. K. Shearer, D. J. Rowland, M. Lerche, C. B. Agee, An earth-like beginning for ancient Mars indicated by alkali-rich volcanism at 4.4 Ga, in *45th Lunar and Planetary Science Conference*, The Woodlands, Texas, 17 to 21 March 2014 (LPSC 2014), Abstract # 1320.
9. J. J. Bellucci, A. A. Nemchin, M. J. Whitehouse, M. Humayun, R. Hewins, B. Zanda, Pb-isotopic evidence for an early, enriched crust on Mars. *Earth Planet. Sci. Lett.* **410**, 34–41 (2015).
10. J. A. Cartwright, U. Ott, S. Herrmann, C. B. Agee, Modern atmospheric signatures in 4.4 Ga Martian meteorite NWA 7034. *Earth Planet. Sci. Lett.* **400**, 77–87 (2014).
11. F. N. Lindsay, J. S. Delaney, B. D. Turrin, G. F. Herzog, J. Park, C. C. Swisher, Ar ages of Martian meteorite NWA 7034, in *47th Lunar and Planetary Science Conference*, The Woodlands, Texas, 21 to 25 March 2016 (LPSC 2016), Abstract # 3013.
12. F. N. Lindsay, B. D. Turrin, C. Göpel, G. F. Herzog, B. Zanda, R. Hewins, J. Park, J. S. Delaney, C. C. Swisher III, $^{40}Ar/^{39}Ar$ ages of Martian meteorite NWA 7533, in *77th Annual Meeting of the Meteoritical Society*, Casablanca, Morocco, 8 to 13 September 2014 (LPI, 2014).
13. W. S. Cassata, P. R. Renne, Systematic variations of argon diffusion in feldspars and implications for thermochronometry. *Geochim. Cosmochim. Acta* **112**, 251–287 (2013).
14. K. A. Farley, (U-Th)/He dating: Techniques, calibrations, and applications. *Rev. Mineral. Geochem.* **47**, 819–844 (2002).
15. Yu. A. Shukolyukov, M. M. Fugzan, I. P. Paderin, S. A. Sergeev, D. P. Krylov, Geothermochronology based on noble gases: I. Stability of the U-Xe isotopic system in nonmetamict zircons. *Petrology* **17**, 1–24 (2009).
16. W. S. Cassata, Meteorite constraints on Martian atmospheric loss and paleoclimate. *Earth Planet. Sci. Lett.* **479**, 322–329 (2017).
17. J. C. Huneke, S. P. Smith, The realities of recoil:^{39}Ar recoil out of small grains and anomalous age patterns in ^{39}Ar-^{40}Ar dating, in *Proceedings of the 7th Lunar Science Conference* (Pergamon Press, 1976), pp. 1987–2008.
18. W. S. Cassata, P. R. Renne, D. L. Shuster, Argon diffusion in pyroxenes: Implications for thermochronometry and mantle degassing. *Earth Planet. Sci. Lett.* **304**, 407–416 (2011).
19. W. S. Cassata, D. L. Shuster, P. R. Renne, B. P. Weiss, Evidence for shock heating and constraints on Martian surface temperatures revealed by $^{40}Ar/^{39}Ar$ thermochronometry of Martian meteorites. *Geochim. Cosmochim. Acta* **74**, 6900–6920 (2010).
20. C. B. Agee, N. V. Wilson, F. M. McCubbin, K. Ziegler, V. J. Polyak, Z. D. Sharp, Y. Asmerom, M. H. Nunn, R. Shaheen, M. H. Thiemens, A. Steele, M. L. Fogel, R. Bowden, M. Glamoclija, Z. Zhang, S. M. Elardo, Unique meteorite from early Amazonian Mars: Water-rich basaltic breccia Northwest Africa 7034. *Science* **339**, 780–785 (2013).
21. G. B. Hudson, B. M. Kennedy, F. A. Podosek, C. M. Hohenberg, The early solar system abundance of ^{244}Pu as inferred from the St. Severin chondrite, in *Lunar and Planetary Science Conference Proceedings*, Houston, Texas, 14 to 18 March 1988 (LPSC 1989), pp. 547–557.
22. G. W. Lugmair, K. Marti, Sm–Nd–Pu timepieces in the Angra dos Reis meteorite. *Earth Planet. Sci. Lett.* **35**, 273–284 (1977).
23. J. H. Jones, The geochemical coherence of Pu and Nd and the $^{244}Pu/^{238}U$ ratio of the early solar system. *Geochim. Cosmochim. Acta* **46**, 1793–1804 (1982).
24. O. Eugster, Th. Michel, Common asteroid break-up events of eucrites, diogenites, and howardites and cosmic-ray production rates for noble gases in achondrites. *Geochim. Cosmochim. Acta* **59**, 177–199 (1995).
25. S. Goderis, A. D. Brandon, B. Mayer, M. Humayun, Ancient impactor components preserved and reworked in martian regolith breccia Northwest Africa 7034. *Geochim. Cosmochim. Acta* **191**, 203–215 (2016).
26. D. D. Bogard, F. Horz, P. H. Johnson, Shock-implanted noble gases: An experimental study with implications for the origin of Martian gases in shergottite meteorites. *J. Geophys. Res. Biogeosci.* **91**, 99–114 (1986).
27. O. Abramov, D. A. Kring, Impact-induced hydrothermal activity on early Mars. *J. Geophys. Res. Planets* **110**, E12S09 (2005).
28. D. J. Cherniak, W. A. Lanford, F. J. Ryerson, Lead diffusion in apatite and zircon using ion implantation and Rutherford backscattering techniques. *Geochim. Cosmochim. Acta* **55**, 1663–1673 (1991).
29. C. J. Hetherington, I. M. Villa, Barium silicates of the Berisal Complex, Switzerland: A study in geochronology and rare-gas release systematics. *Geochim. Cosmochim. Acta* **71**, 3336–3347 (2007).
30. S. J. Robbins, G. Di Achille, B. M. Hynek, The volcanic history of Mars: High-resolution crater-based studies of the calderas of 20 volcanoes. *Icarus* **211**, 1179–1203 (2011).
31. S. C. Werner, The global martian volcanic evolutionary history. *Icarus* **201**, 44–68 (2009).
32. B. E. Cohen, D. F. Mark, W. S. Cassata, M. R. Lee, T. Tomkinson, C. L. Smith, Taking the pulse of Mars via dating of a plume-fed volcano. *Nat. Commun.* **8**, 640 (2017).
33. N. Artemieva, B. Ivanov, Launch of martian meteorites in oblique impacts. *Icarus* **171**, 84–101 (2004).
34. K. Min, A. E. Farah, S. R. Lee, J. I. Lee, (U-Th)/He ages of phosphates from Zagami and ALHA77005 Martian meteorites: Implications to shock temperatures. *Geochim. Cosmochim. Acta* **196**, 160–178 (2017).
35. S. P. Schwenzer, J. Fritz, D. Stöffler, M. Trieloff, M. Amini, A. Greshake, S. Herrmann, K. Herwig, K. P. Jochum, R. K. Mohapatra, B. Stoll, U. Ott, Helium loss from Martian meteorites mainly induced by shock metamorphism: Evidence from new data and a literature compilation. *Meteorit. Planet. Sci.* **43**, 1841–1859 (2008).
36. J. Fritz, N. Artemieva, A. Greshake, Ejection of Martian meteorites. *Meteorit. Planet. Sci.* **40**, 1393–1411 (2005).
37. I. Leya, J. Masarik, Cosmogenic nuclides in stony meteorites revisited. *Meteorit. Planet. Sci.* **44**, 1061–1086 (2009).
38. R. Trappitsch, A. S. G. Roth, I. Leya, Modeling solar cosmic ray induced cosmogenic nuclides in small meteoroids, in *47th Lunar and Planetary Science Conference*, The Woodlands, Texas, 21 to 25 March 2016 (LPSC 2016), Abstract # 2658.
39. R. Wieler, L. Huber, H. Busemann, S. Seiler, I. Leya, C. Maden, J. Masarik, M. M. M. Meier, K. Nagao, R. Trappitsch, A. J. Irving, Noble gases in 18 Martian meteorites and angrite Northwest Africa 7812—Exposure ages, trapped gases, and a re-evaluation of the evidence for solar cosmic ray-produced neon in shergottites and other achondrites. *Meteorit. Planet. Sci.* **51**, 407–428 (2016).
40. A. S. G. Roth, R. Trappitsch, K. Metzler, B. A. Hofmann, I. Leya, Neon produced by solar cosmic rays in ordinary chondrites. *Meteorit. Planet. Sci.* **52**, 1155–1172 (2017).
41. D. O. Revelle, A quasi-simple ablation model for large meteorite entry: Theory vs observations. *J. Atmos. Terr. Phys.* **41**, 453–473 (1979).
42. T. R. Watters, P. J. McGovern, R. P. Irwin III, Hemispheres apart: The crustal dichotomy on Mars. *Annu. Rev. Earth Planet. Sci.* **35**, 621–652 (2007).
43. M. M. Marinova, O. Aharonson, E. Asphaug, Mega-impact formation of the Mars hemispheric dichotomy. *Nature* **453**, 1216–1219 (2008).
44. F. Nimmo, S. D. Hart, D. G. Korycansky, C. B. Agnor, Implications of an impact origin for the martian hemispheric dichotomy. *Nature* **453**, 1220–1223 (2008).

45. G. Leone, P. J. Tackley, T. V. Gerya, D. A. May, G. Zhu, Three-dimensional simulations of the southern polar giant impact hypothesis for the origin of the Martian dichotomy. *Geophys. Res. Lett.* **41**, 8736–8743 (2014).
46. C. C. Reese, C. P. Orth, V. S. Solomatov, Impact origin for the Martian crustal dichotomy: Half emptied or half filled? *J. Geophys. Res. Planets* **115**, E05004 (2010).
47. C. C. Reese, C. P. Orth, V. S. Solomatov, Impact megadomes and the origin of the martian crustal dichotomy. *Icarus* **213**, 433–442 (2011).
48. C. C. Reese, V. S. Solomatov, Fluid dynamics of local martian magma oceans. *Icarus* **184**, 102–120 (2006).
49. R. I. Citron, S. Zhong, Constraints on the formation of the Martian crustal dichotomy from remnant crustal magnetism. *Phys. Earth Planet. In.* **212**, 55–63 (2012).
50. R. Brasser, S. J. Mojzsis, A colossal impact enriched Mars' mantle with noble metals. *Geophys. Res. Lett.* **44**, 5978–5985 (2017).
51. T. Keller, P. J. Tackley, Towards self-consistent modeling of the martian dichotomy: The influence of one-ridge convection on crustal thickness distribution. *Icarus* **202**, 429–443 (2009).
52. S. C. Solomon, O. Aharonson, J. M. Aurnou, W. B. Banerdt, M. H. Carr, A. J. Dombard, H. V. Frey, M. P. Golombek, S. A. Hauck II, J. W. Head III, B. M. Jakosky, C. L. Johnson, P. J. McGovern, G. A. Neumann, R. J. Phillips, D. E. Smith, M. T. Zuber, New perspectives on ancient Mars. *Science* **307**, 1214–1220 (2005).
53. S. Zhong, M. T. Zuber, Degree-1 mantle convection and the crustal dichotomy on Mars. *Earth Planet. Sci. Lett.* **189**, 75–84 (2001).
54. O. Šrámek, S. Zhong, Martian crustal dichotomy and Tharsis formation by partial melting coupled to early plume migration. *J. Geophys. Res. Planets* **117**, E01005 (2012).
55. L. T. Elkins-Tanton, P. C. Hess, E. M. Parmentier, Possible formation of ancient crust on Mars through magma ocean processes. *J. Geophys. Res. Planets* **110**, E12S01 (2005).
56. W. K. Hartmann, G. Neukum, Cratering chronology and the evolution of Mars. *Space Sci. Rev.* **96**, 165–194 (2001).
57. P. Beck, A. Pommerol, B. Zanda, L. Remusat, J. P. Lorand, C. Göpel, R. Hewins, S. Pont, E. Lewin, E. Quirico, B. Schmitt, G. Montes-Hernandez, A. Garenne, L. Bonal, O. Proux, J. L. Hazemann, V. F. Chevrier, A Noachian source region for the "Black Beauty" meteorite, and a source lithology for Mars surface hydrated dust? *Earth Planet. Sci. Lett.* **427**, 104–111 (2015).
58. H. V. Frey, J. H. Roark, K. M. Shockey, E. L. Frey, S. E. H. Sakimoto, Ancient lowlands on Mars. *Geophys. Res. Lett.* **29**, 22-1–22-4 (2002).
59. G. A. Neumann, M. T. Zuber, M. A. Wieczorek, P. J. McGovern, F. G. Lemoine, D. E. Smith, Crustal structure of Mars from gravity and topography. *J. Geophys. Res. Planets* **109**, E08002 (2004).
60. A. S. McEwen, M. C. Malin, M. H. Carr, W. K. Hartmann, Voluminous volcanism on early Mars revealed in Valles Marineris. *Nature* **397**, 584–586 (1999).
61. C. M. Hohenberg, K. Marti, F. A. Podosek, R. C. Reedy, J. R. Shirck, Comparisons between observed and predicted cosmogenic noble gases in lunar samples, in *Lunar and Planetary Science Conference, 9th, Houston, Texas, March 13–17, 1978, Proceedings* (Pergamon Press Inc., 1978), vol. 2, pp. 2311–2344.
62. E. C. Alexander Jr., R. S. Lewis, J. H. Reynolds, M. C. Michel, Plutonium-244: Confirmation as an extinct radioactivity. *Science* **172**, 837–840 (1971).
63. W. S. Cassata, L. E. Borg, A new approach to cosmogenic corrections in $^{40}Ar/^{39}Ar$ chronometry: Implications for the ages of Martian meteorites. *Geochim. Cosmochim. Acta* **187**, 279–293 (2016).
64. W. S. Cassata, P. R. Renne, D. L. Shuster, Argon diffusion in plagioclase and implications for thermochronometry: A case study from the Bushveld Complex, South Africa. *Geochim. Cosmochim. Acta* **73**, 6600–6612 (2009).
65. M. C. Croarkin, W. F. Guthrie, G. W. Burns, M. Kaeser, G. F. Strouse, *Temperature-Electromotive Force Reference Functions and Tables for the Letter-Designated Thermocouple Types Based on the ITS-90* (National Institute of Standards and Technology Monograph 175, NIST, 1993), 642 pp.
66. J. Eikenberg, P. Signer, R. Wieler, U-Xe, U-Kr, and U-Pb systematics for dating uranium minerals and investigations of the production of nucleogenic neon and argon. *Geochim. Cosmochim. Acta* **57**, 1053–1069 (1993).
67. G. R. Eppich, K. B. Knight, T. W. Jacomb-Hood, G. D. Spriggs, I. D. Hutcheon, Constraints on fallout melt glass formation from a near-surface nuclear test. *J. Radioanal. Nucl. Chem.* **302**, 593–609 (2014).
68. P. R. Fields, A. M. Friedman, J. Milsted, J. Lerner, C. M. Stevens, D. Metta, W. K. Sabine, Decay properties of plutonium-244, and comments on its existence in nature. *Nature* **212**, 131–134 (1966).
69. A. M. Gaffney, A. Hubert, W. S. Kinman, M. Magara, A. Okubo, F. Pointurier, K. C. Schorzman, R. E. Steiner, R. W. Williams, Round-robin ^{230}Th–^{234}U age dating of bulk uranium for nuclear forensics. *J. Radioanal. Nucl. Chem.* **307**, 2055–2060 (2016).
70. D. Heymann, On the origin of hypersthene chondrites: Ages and shock effects of black chondrites. *Icarus* **6**, 189–221 (1967).
71. A. H. Jaffey, K. F. Flynn, L. E. Glendenin, W. C. Bentley, A. M. Essling, Precision measurement of half-lives and specific activities of 235U and 238U. *Phys. Rev. C* **4**, 1889–1906 (1971).
72. K. P. Jochum, U. Weis, B. Schwager, B. Stoll, S. A. Wilson, G. H. Haug, M. O. Andreae, J. Enzweiler, Reference values following ISO guidelines for frequently requested rock reference materials. *Geostand. Geoanal. Res.* **40**, 333–350 (2016).
73. J.-Y. Lee, K. Marti, J. P. Severinghaus, K. Kawamura, H.-S. Yoo, J. B. Lee, J. S. Kim, A redetermination of the isotopic abundances of atmospheric Ar. *Geochim. Cosmochim. Acta* **70**, 4507–4512 (2006).
74. J. P. Lorand, R. H. Hewins, L. Remusat, B. Zanda, S. Pont, H. Leroux, M. Marinova, D. Jacob, M. Humayun, A. Nemchin, M. Grange, A. Kennedy, C. Göpel, Nickeliferous pyrite tracks pervasive hydrothermal alteration in Martian regolith breccia: A study in NWA 7533. *Meteorit. Planet. Sci.* **50**, 2099–2120 (2015).
75. K. R. Ludwig, *User's Manual for Isoplot 3.00: A Geochronological Toolkit for Microsoft Excel* (Kenneth R. Ludwig, 2003).
76. A. Meshik, C. Hohenberg, O. Pravdivtseva, D. Burnett, Heavy noble gases in solar wind delivered by Genesis mission. *Geochim. Cosmochim. Acta* **127**, 326–347 (2014).
77. A. A. Nemchin, M. Humayun, M. J. Whitehouse, R. H. Hewins, J.-P. Lorand, A. Kennedy, M. Grange, B. Zanda, C. Fieni, D. Deldicque, Record of the ancient martian hydrosphere and atmosphere preserved in zircon from a martian meteorite. *Nat. Geosci.* **7**, 638–642 (2014).
78. P. R. Renne, G. Balco, K. R. Ludwig, R. Mundil, K. Min, Response to the comment by W.H. Schwarz et al. on "Joint determination of ^{40}K decay constants and $^{40}Ar^*/^{40}K$ for the Fish Canyon sanidine standard, and improved accuracy for $^{40}Ar/^{39}Ar$ geochronology" by P.R. Renne et al. (2010). *Geochim. Cosmochim. Acta* **75**, 5097–5100 (2011).
79. P. R. Renne, A. L. Deino, F. J. Hilgen, K. F. Kuiper, D. F. Mark, W. S. Mitchell III, L. E. Morgan, R. Mundil, J. Smit, Time scales of critical events around the Cretaceous-Paleogene boundary. *Science* **339**, 684–687 (2013).
80. R. W. Williams, A. M. Gaffney, ^{230}Th-^{234}U model ages of some uranium standard reference materials. *Proceedings in Radiochemistry A Supplement to Radiochimica Acta* **1**, 31–35 (2011).
81. T. Yoshioka, T. Tsuruta, H. Iwano, T. Danhara, Spontaneous fission decay constant of ^{238}U determined by SSNTD method using CR-39 and DAP plates. *Nucl. Instrum. Methods Phys. Res., Sect. A* **555**, 386–395 (2005).
82. K. Thirumalai, A. Singh, R. Ramesh, A MATLAB™ code to perform weighted linear regression with (correlated or uncorrelated) errors in bivariate data. *J. Geol. Soc. India* **77**, 377–380 (2011).

Acknowledgments: We thank two anonymous reviewers for thoughtful and constructive reviews that significantly improved the manuscript. **Funding:** This work was performed under the auspices of the U.S. Department of Energy by LLNL under contract DE-AC52-07NA27344. Financial support was provided by the NASA Mars Fundamental Research Program (grant NNH14AX56I to W.S.C.) and an LLNL Laboratory Directed Research and Development project (17-ERD-001), "Uncovering the Origins of the Solar System with Cosmochemical Forensics." C. Agee (University of New Mexico) is thanked for the provision of samples to LLNL. D. Pitt is thanked for assistance in purchasing the sample that was used for SUERC analyses. The UK work component was funded by the Science and Technology Facilities Council (grants ST/H002472/1, ST/H002960/1, and ST/K000918/1 to D.F.M. and M.R.L.). NERC is thanked for continued funding of the Argon Isotope Facility at SUERC. R. Dymock and J. Imlach (SUERC) and L. Hallis and P. Chung (Glasgow) are thanked for technical assistance with $^{40}Ar/^{39}Ar$ and scanning electron microscopy, respectively. **Author contributions:** W.S.C., B.E.C., M.R.L., and C.L.S. were primarily responsible for sample selection and characterization. W.S.C., B.E.C., D.F.M., and C.A.C. performed the noble gas analyses. J.W. performed the ICP-MS analyses. R.T. performed the cosmogenic nuclide modeling. W.S.C., B.E.C., and D.F.M. interpreted the data and wrote the paper, with input from all the other authors. **Competing interests:** The authors declare that they have no competing interests. **Data and materials availability:** All data needed to evaluate the conclusions in the paper are present in the paper and/or the Supplementary Materials. Additional data related to this paper may be requested from the authors.

Submitted 30 August 2017
Accepted 10 April 2018
Published 23 May 2018
10.1126/sciadv.aap8306

Citation: W. S. Cassata, B. E. Cohen, D. F. Mark, R. Trappitsch, C. A. Crow, J. Wimpenny, M. R. Lee, C. L. Smith, Chronology of martian breccia NWA 7034 and the formation of the martian crustal dichotomy. *Sci. Adv.* **4**, eaap8306 (2018).

Science Advances

Chronology of martian breccia NWA 7034 and the formation of the martian crustal dichotomy

William S. Cassata, Benjamin E. Cohen, Darren F. Mark, Reto Trappitsch, Carolyn A. Crow, Joshua Wimpenny, Martin R. Lee and Caroline L. Smith

Sci Adv **4** (5), eaap8306.
DOI: 10.1126/sciadv.aap8306